

Emergent Universal Drag Law in a Model of Superflow

M.T.M. Christenhusz,¹ A. Safavi-Naini,² H. Rubinsztein-Dunlop,¹ T.W. Neely,¹ and M.T. Reeves³

¹*Australian Research Council Centre of Excellence for Engineered Quantum Systems,*

School of Mathematics and Physics, University of Queensland, St. Lucia, QLD 4072, Australia.

²*Institute of Physics, University of Amsterdam, Science Park 904, 1098 XH Amsterdam, the Netherlands.*

³*Australian Research Council Centre of Excellence in Future Low-Energy Electronics Technologies,*
School of Mathematics and Physics, University of Queensland, St Lucia, QLD 4072, Australia.

(Dated: June 21, 2024)

Despite the fundamentally different dissipation mechanisms, many laws and phenomena of classical turbulence equivalently manifest in quantum turbulence. The Reynolds law of dynamical similarity states that two objects of same geometry across different length scales are hydrodynamically equivalent under the same Reynolds number, leading to a universal drag coefficient law. In this work we confirm the existence of a universal drag law in a superfluid wake, facilitated by the nucleation of quantized vortices. We numerically study superfluid flow across a range of Reynolds numbers for the paradigmatic classical hard-wall and the Gaussian obstacle, popular in experimental quantum hydrodynamics. In addition, we provide a feasible method for measuring superfluid drag forces in an experimental environment using control volumes.

The principle of dynamical similarity is a cornerstone of classical fluid dynamics that allows problems to be cast in terms of dimensionless parameters. This principle is not just a useful heuristic of dimensional analysis but is intimately tied to the scale invariance of the governing equations, revealing underlying universality of different flow phenomena. Two physical situations are guaranteed to be identical under appropriate scaling of space and time only if all relevant control parameters are the same [1, 2]. The Reynolds number, Re , is perhaps the most ubiquitous control parameter, governing the transition from laminar (smooth) to turbulent (vorticity dominated) flows. The Reynolds number for flow velocity u , characteristic length D , and kinematic viscosity ν , is given by $Re = uD/\nu$, and measures the ratio of inertia to viscosity, characterising the degree of turbulent motion.

Superfluid turbulence displays significant similarities to its classical counterpart. These include the persistence of the celebrated Kolmogorov law [3–5], the same value of the Kolmogorov constant, and the existence of the dissipation anomaly [6, 7]. Moreover, in a superfluid the vortex dynamics are governed by the Kirchoff/Biot-Savart equations, which remain invariant under the same scaling transform as the Navier-Stokes equations [8, 9]. Beyond these examples relevant to high Reynolds numbers, the similarities extend further still; for example, the von Kármán street — a moderate Reynolds number phenomenon — emerges in the wake of a bluff body in a pure superfluid [10, 11]. These similarities suggest that an appropriate Reynolds number should emerge in the pure superfluid. However, superfluids differ from ordinary fluids in three major respects: i) their viscosity $\nu = 0$ identically; ii) vorticity may only be introduced with discrete circulation $\Gamma = 2\pi\hbar/m$, and iii) vorticity may only appear above a critical velocity u_c . Thus any Reynolds number should account for the close connection between vortex shedding and effective viscosity of the su-

perfluid once the flow velocity surpasses a critical velocity u_c . As noted by Onsager, circulation quantum has the same dimensions as ν suggesting $Re_S \sim uD/\kappa$, with $\kappa = h/m$ [12]. In Ref. [13] it was shown that when accounted for the critical velocity, the “superfluid Reynolds number” $Re_S = (u - u_c)D/\kappa$ [14], revealed similarity in the vortex shedding frequency behind a Gaussian-shaped obstacle and was subsequently utilized to characterize intermittent turbulence in superfluid He-II [15]. However, to establish dynamical similarity through this superfluid Reynolds number we must first answer fundamental open questions: i) are *all* relevant dimensionless quantities expressible as a universal function of Re_S ? and ii) is the universality robust to the system details embedded within u_c ? [16].

In this Letter we address this gap by numerically investigating the drag force, F_d , experienced by different obstacles within a 2D superflow within the Gross-Pitaevskii model. We identify different regimes of drag associated with differing regimes of vortex shedding and investigate the drag coefficient C_d . Next, we study the flow across a range of Reynolds numbers for several obstacles. We account for the dependence of u_c on the obstacle shape to extract a universal relation for C_d . Finally, we introduce an experimental method for measuring F_d in current platforms which will allow for the confirmation of the universal relations obtained here.

We consider the flow of a 2D superfluid past an obstacle, modelling by the Gross-Pitaevskii equation (GPE). In the frame where the obstacle is moving through the superfluid at velocity \mathbf{u} , the equation of motion is:

$$i\hbar \frac{\partial \psi(\mathbf{r}, t)}{\partial t} = (\mathcal{L} - \mathbf{u} \cdot \mathbf{p} - \mu) \psi(\mathbf{r}, t), \quad (1)$$

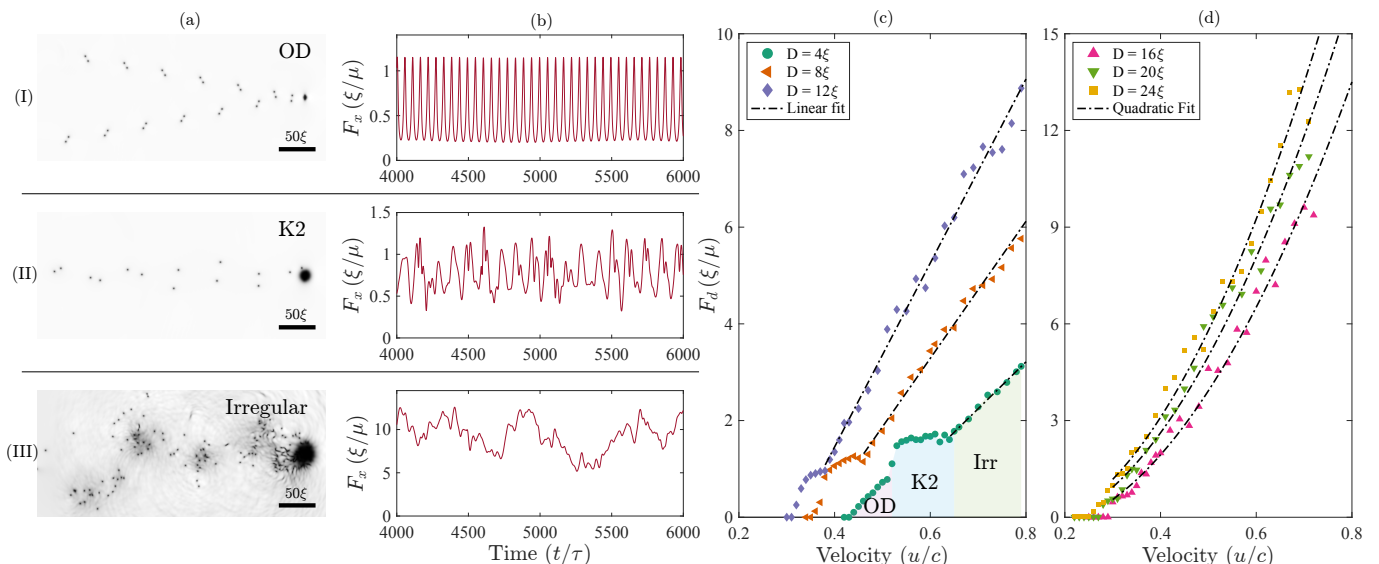


FIG. 1. (a) The three vortex shedding regimes (OD, K2, Irregular) in superfluid wakes with (b) corresponding longitudinal force time series for a Gaussian obstacle of width $D = 4\xi$ (I), $D = 12\xi$ (II) and $D = 24\xi$ (III). Panel (c) depicts the mean of the steady state force-time series for obstacle sizes, 4ξ , 8ξ and 12ξ . For these small obstacle sizes, the different shedding regimes can be observed and drag scales linearly (dashed fits). (d) Upon increasing the obstacle size and Reynolds number, quadratic drag scaling emerges (dashed guidelines) for obstacle sizes 16ξ , 20ξ and 24ξ .

where μ is the chemical potential, $\mathbf{p} = -i\hbar\nabla$, and

$$\mathcal{L}\psi(\mathbf{r}, t) \equiv \left[-\frac{\hbar^2}{2m}\nabla^2 + V(\mathbf{r}) + g_2|\psi(\mathbf{r}, t)|^2 \right] \psi(\mathbf{r}, t). \quad (2)$$

Here $V(\mathbf{r})$ is functional form of the obstacle, and g_2 is an effective 2D interaction strength. We work in natural units of the healing length ξ , and time τ , where we set $\mu = 1$.

The drag force F_d may be calculated from the Ehrenfest relation, $F_x(t) = -\int d^2\mathbf{r} \psi^*(\mathbf{r}, t)(\partial_x V(\mathbf{r}))\psi(\mathbf{r}, t)$, which may then be averaged over time once the system reaches a steady state: $F_d = \langle F_x(t) \rangle$. To achieve steady state wakes we implement the fringe method introduced in Ref. [13], which adds a damping layer $\gamma(\mathbf{r})$ at the edge of the domain, and deletes vortices within the fringe region using a phase imprinting technique [17]. This allows recycling of the flow on periodic boundary conditions, and facilitates the long-time simulations required to accurately resolve the drag force.

This modifies Eq. (1) to

$$i\hbar\frac{\partial\psi(\mathbf{r}, t)}{\partial t} = (\mathcal{L} - \mathbf{u} \cdot \mathbf{p} - \mu)\psi(\mathbf{r}, t) - i\gamma(\mathbf{r})(\mathcal{L}_f - \mu)\psi(\mathbf{r}, t), \quad (3)$$

where $\mathcal{L}_f \equiv \mathcal{L} - V(\mathbf{r})$. The damping rate $\gamma(\mathbf{r})$ is ramped up smoothly from zero across the interface between the computational region and the fringe region to prevent reflections.

We first investigate the drag force for flow past a Gaussian obstacle, $V_G(\mathbf{r}) = V_0 \exp(-r^2/\sigma^2)$, as a function of the obstacle size. Gaussian obstacles are most readily

available to experiments, being implemented with a focused optical beam [18–20]. The vortex shedding regimes were identified in Ref. [10] and are also shown in Figure 1(a): (I) the oblique dipole (OD), (II) the charge-2 von Kármán shedding (K2), and (III) irregular shedding. Their corresponding longitudinal force time series are plotted in (b). For superfluids, shedding becomes sufficiently irregular (III), corresponding to the transition to fully developed turbulence in the wake of the barrier, beyond $\text{Re}_S \sim 0.7$ [13]. The drag force (see Figure 1 (III,b)) time series resembles that of turbulent flow in this regime.

Panels (c) and (d) of Figure 1 show the drag force as a function of the superfluid velocity for a range of Gaussian obstacle sizes. In the OD regime, the drag force is dominated by the quantum vortex dipole momentum [21] and increases linearly with the shedding frequency. In the K2 regime, two same-sign vortices shed from the top or the bottom of the barrier (Fig. 1(II)). Shedding of a doublet occurs – contrary to OD shedding – out of phase between the top and the bottom of the barrier. The rapid shedding of a same-sign vortex pair results in a majority of the force being exerted into the transverse direction, resulting in a decreased linear gradient for the drag force, depicted in the shaded area labelled as “K2” in Fig. 1(c). The shaded area labelled as “Irr” depicts the irregular shedding regime for the Gaussian barrier. Beyond $\text{Re}_S \sim 0.7$, K2 shedding is unstable and shedding occurs irregularly and at a large frequency, causing clusters of vortices to form. The drag force increases at a faster rate in this regime.

The panels (c) and (d) also illustrate a qualitative dif-

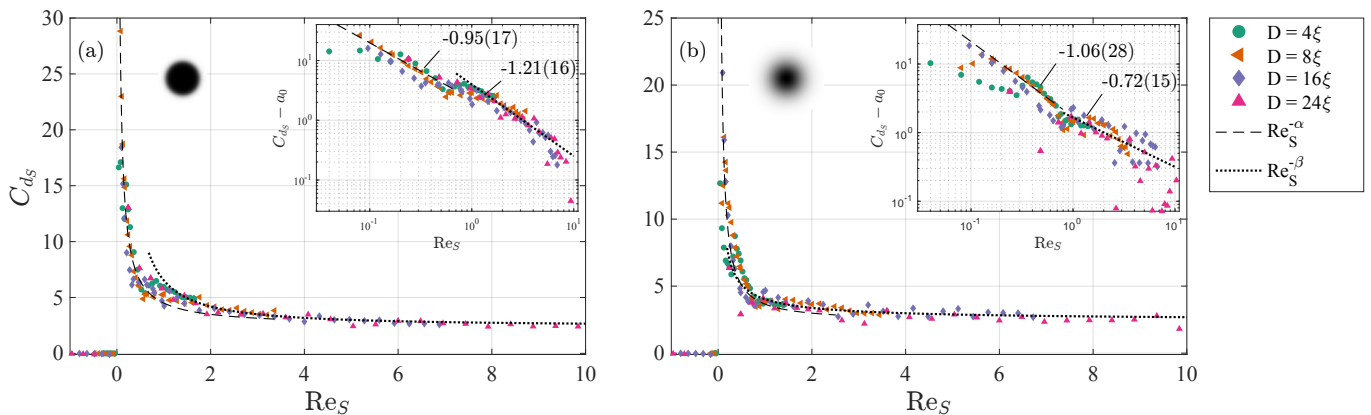


FIG. 2. Drag coefficient as a function of the Reynolds number for a (a) hard walled and (b) Gaussian obstacle. Data points of one colour/shape correspond to a constant obstacle size at different wake velocities. The collapse of data points of different obstacle sizes onto a single curve illustrate the presence of the dynamical similarity for superfluidic drag. The log-log insets plot $C_{d_S} - a_0 \sim C_{d_S} - C_{d_S}(Re_S \simeq \infty)$ as a function of Re_S and reveal power laws for both obstacles corresponding $\alpha = 0.95(17)$ and $\beta = 1.21(16)$ for the hard walled obstacle, and $\alpha = 1.06(28)$ and $\beta = 0.72(15)$ for the Gaussian barrier. The outliers at small Reynolds number correspond to the quantum exclusive OD shedding regime and are not considered for the dynamical similarity.

ference in the shedding behaviour of small and large obstacles: (i) for increasingly larger obstacle sizes, the OD and K2 regime are unstable, thus absent, and irregular shedding starts immediately for $u > u_c$ (Fig. 1d), and (ii) the drag force scales quadratically with the flow velocity, $F_d \sim u^2$. This quadratic scaling emerges due to the large number of vortex-vortex interactions around the barrier, which start to significantly affect the shedding and become the main component of the drag force. By contrast, for sufficiently small obstacles, the drag force is well described by the dipole momentum and provides the largest contribution to the drag, which is linear with u .

Next we probe the Reynolds law of dynamical similarity for superfluidic drag by repeating the numerical studies presented in Figure 1 for different obstacle sizes and shapes and in each case extract the dimensionless drag coefficient C_{d_S} as a function of the superfluid Reynolds number. The dimensionless drag coefficient expresses the momentum transfer of a fluid with an object of a particular geometry, independent of object size, fluid velocity and density, thus allowing us to extract the universal drag scaling law. The drag coefficient is given by $C_{d_S} = 2F_d/\rho(u^2 - u_c^2)D$, where we have modified the usual definition of the drag coefficient [22] to account for the absence of drag in a superfluid below the critical velocity u_c (see Supplementary S2).

Figure 2 depicts the drag coefficient as a function of the Reynolds number for (a) a hard-wall circular barrier and (b) a Gaussian barrier. The collapse of the data points corresponding to different obstacle sizes onto a single curve is clear evidence of the dynamical similarity for superfluidic drag, with similar qualitative features as reported for those in classical hydrodynamics [23, 24]. To extract an empirical expression for the drag similitude

of a particular geometry, we use the procedure used in classical hydrodynamics where the drag coefficient across different flow regimes is fit by a functional form [25]

$$C_d = a_1 Re^{-\alpha} + a_2 Re^{-\beta} + a_0, \quad (4)$$

with α corresponding to the scaling in the low Re limit, β at an intermittent region and a_0 corresponding to the inertial asymptotic regime at $C_d(Re \rightarrow \infty) = a_0$. Note the persistence of the dissipation anomaly in superfluids suggests $a_0 > 0$ [2, 7, 26].

To prevent overparametrization, we fit α and β in three steps: (i) a_0 is obtained by taking the mean of the last five datapoints. At this point, the curve is sufficiently flat with a sufficiently low standard error. (ii) To find α (β), a_2 (a_1) is set to zero. (iii) α is found at $Re_S < 0.7$, β is obtained for $Re_S > 0.7$ on a log-log plot with $C_{d_S} - a_0$ as a function of Re_S . Outliers at low Reynolds numbers correspond to the superfluid unique OD vortex shedding regime and are not part of the similitude. Outliers at large Reynolds numbers are introduced artificially through subtracting a_0 and not considered in fitting of the power laws. Log-log plots in which a_0 is not subtracted is found in the Supplementary Sec. S3.

The main source of error in our fits is the confidence in estimation of the asymptotic constant, a_0 , which we extract from our numerical simulations. This is due to the limited range of computationally accessible Reynolds numbers; a large range is required to demonstrate the fully inertial regime at which a_0 may be obtained with higher confidence.

A number of striking parallels exist between the quantum and classical dynamic similarity. At low Re, the classical sphere and cylinder obstacles' drag coefficient

follow $C_d \approx \text{Re}^{-1}$, i.e. $\alpha = -1$. [27–29], similar to the superfluidic hard wall and Gaussian obstacles, with $\alpha = 0.95(17)$ and $1.06(28)$, respectively (see inset of Fig. 2). The underlying mechanisms causing this power law are vastly different, with the classical α originating from time-reversible Stokes flow. In contrast, below the speed of sound, ($u \ll c$), superfluidic drag originates almost exclusively from time-irreversible vortex nucleation dominated by the quantum dipole force [30]. The power laws at larger Re_S correspond to $\beta = 1.21(16)$ and $0.72(15)$ for the hard wall and Gaussian respectively, and are the result of more complex vortex dynamics. We believe that – analogous to classical hydrodynamics – this regime is dominated by boundary layer effects [31–34].

In addition to the hard-wall circular and Gaussian obstacle, we investigated the the asymptotic a_0 value for non-trivial obstacle shapes. In classical hydrodynamics, a_0 is the number associated with an object’s ‘constant’ drag coefficient and quantifies the aerodynamicity of an object’s shape. Table I summarizes the constant drag coefficient for a flat plate, wedge, and airfoil-shaped obstacle and compares it to the classical values. These have been extracted using the same procedure as those of the Gaussian and hard-wall obstacles. Drag coefficient curves for these obstacles are found in Supplementary Sec. S2. We remark the stark difference between the classical and superfluid airfoil. While the drag coefficient is remarkably lower than other obstacles, the difference is much less pronounced than for classical obstacles.

Next, we outline how the universality of the drag coefficient can be verified experimentally. Here, we must consider the limited resolution with which we are able to probe the superfluid wake. This means that the procedure used in our numerical simulations, based on the Ehrenfest relation, cannot be directly applied experimentally. Instead we note that in an otherwise unperturbed flow, drag force may equivalently be obtained by considering the total momentum flow in a set volume around an obstacle.

The first step is to cast the system into a control volume, as described in classical hydrodynamics [36, 37], using the Leibniz-Reynolds transport theorem [38]:

		Classical (C_d)	Quantum (C_{d_S})
Wedge		2.00	1.93(6)
Flat plate		1.98	2.14(5)
Circle		1.17	2.40(6)
Gaussian		N/A	2.37(16)
Airfoil		0.09	1.57(8)

TABLE I. Drag coefficients at $C_d(\text{Re} \rightarrow \infty)$ in classical and quantum systems. The Gaussian obstacle has no trivial classical analog. Classical drag coefficients obtained from [22, 35].

$$\frac{\partial(m\mathbf{u})_{\text{sys}}}{\partial t} = \frac{\partial}{\partial t} \int_{\text{CV}} \rho\mathbf{u} dV + \int_{\text{CS}} \rho\mathbf{u}(\mathbf{u} \cdot \mathbf{n}) dA, \quad (5)$$

where the left hand side is the momentum flux of a closed system, CV is a control volume around the obstacle, and CS is the perimeter of the control volume. Here ρ and \mathbf{u} represent the density and velocity of the fluid inside the control volume, respectively, and \mathbf{n} the normal vector pointing out of the control surface. The first term on the right-hand side is the change of total momentum inside the control volume in time, which vanishes in steady state with constant inflow velocity and density, and the second term on the right-hand side is the net flow of momentum through the control volume boundary.

Next, we rewrite Eq. (5) in the quantum hydrodynamics approximation by replacing the density $\rho \rightarrow m\psi^*\psi$, and $\rho\mathbf{u} \rightarrow \mathbf{J} = \frac{-i\hbar}{2}(\psi^*\nabla\psi - \psi\nabla\psi^*)$ [39]. For a two-dimensional system the resulting expression for the the net force acting on the control area, or the momentum flux, is given by

$$\frac{\partial}{\partial t} \iint_{\Omega} \mathbf{J} d\Omega + \oint_{\Gamma} \mathbf{J}(\mathbf{u} \cdot \mathbf{n}) dl = \oint_{\Gamma} T_{jk} dl - \iint_{\Omega} \rho\partial_k \left(\frac{V}{m} \right) d\Omega, \quad (6)$$

where Ω is the two-dimensional control area, Γ is the surface encompassing the control area, and T_{jk} is the momentum flux density tensor [30]. The last term is the Ehrenfest relation in the hydrodynamic limit, with ∂_k the spatial derivative in k and V the potential and m the mass [39].

In the steady state and for sufficiently smooth obstacles, where the above equation can be further simplified to

$$\oint_{\Gamma} \mathbf{J}(\mathbf{u} \cdot \mathbf{n}) dl = - \iint_{\Omega} \rho\partial_k \left(\frac{V}{m} \right) d\Omega,$$

the force in direction k may be evaluated using the Ehrenfest relation, or by considering the momentum current density flowing through a control surface around an obstacle. This control volume method introduced here has great experimental utility as the largest contributions to the Ehrenfest relation occur within a number of healing lengths around the obstacle, requiring large experimental resolution to obtain the drag force accurately.

We have analyzed the data from Fig. 1(c,d) using the two methods, with the results are plotted in Fig. 3. We limit the the downstream boundary to be no further than $L_y/2$ away from the obstacle to prevent contributions from edge effects in our finite-sized grid. We compare the method for small (left) and large (right) obstacles, for both the hard wall (green dots) and Gaussian (orange triangles) barriers. The filled data points correspond to the Ehrenfest method, with corresponding shaded areas for the error. Due to long time correlations, the error is equivalent to the standard deviation of the force time series (depicted in Fig. 1(b)).

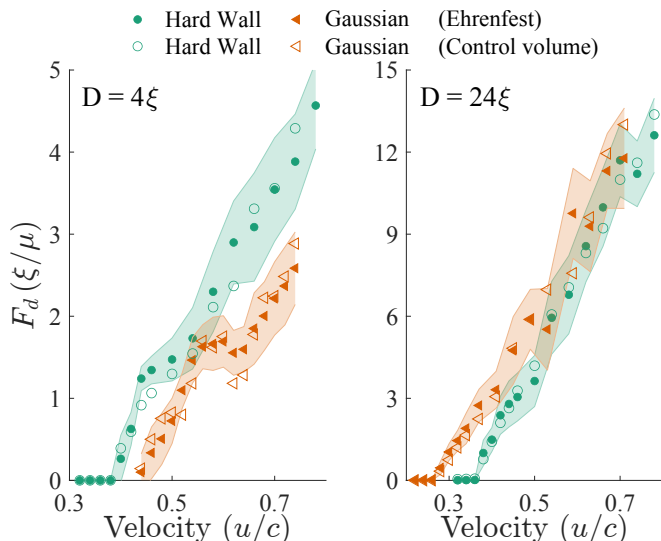


FIG. 3. Drag force for a hard wall (circle) and Gaussian (triangle) obstacle, obtained from the longitudinal force time series using the Ehrenfest relation (filled datapoints) and control volume method (open dots). Shaded areas represent the error on the Ehrenfest method.

Open data points are obtained through the control volume method. Across the range of all our independent parameters, the control volume method is in good agreement with the Ehrenfest method, showing the effectiveness of this method. This method will open up new in situ techniques for measuring superfluid drag in Bose-Einstein condensates: Experimental verification is realisable for superfluids with access to the velocity field, such as atomic Bose-Einstein condensate experiments utilising Bragg spectroscopy [40, 41].

In conclusion, we have confirmed the existence of the Reynolds law of similarity for superfluidic drag. Existence of the drag similtude provides further evidence of the utility of the superfluid Reynolds number. Our results, and the earlier demonstrated universal behaviour for the Strouhal number [13], suggest *all* relevant dimensionless quantities are expressible as a universal function of the Re_S due to scale invariance. In addition, we investigated the drag coefficient of various bluff and streamlined obstacles and found significant differences with a significantly higher drag coefficient for a streamlined airfoil than its classical equivalent. Finally, we provide an alternative method of obtaining the drag force in a wake which opens up the ability for experimental measurements of superfluidic drag. Future work at larger Reynolds numbers, realised at much larger computational grids, can shed new light on constant drag coefficients and the dissipation anomaly in superfluids.

ACKNOWLEDGEMENTS

We thank G. Gauthier for the valuable discussions. This research was supported by the Australian Research Council (ARC) Centre of Excellence for Engineered Quantum Systems (EQUS Grant No. CE170100009), and ARC Future Fellowship FT190100306. M.T.M.C. acknowledges the support of an Australian Government Research and Training Program Scholarship. A.S.N. is supported by the Dutch Research Council (NWO/OCW), as part of the Quantum Software Consortium programme (project number 024.003.037) and Quantum Delta NL (project number NGF.1582.22.030), T.W.N. acknowledges the support of Australian Research Council Future Fellowship No. FT190100306. M.T.R. acknowledges the support of an Australian Research Council Discovery Early Career Research Award DE220101548. Computing support was provided by the Getafix cluster at the University of Queensland.

- [1] G. K. Batchelor, Dynamical similarity and the Reynolds number, in *An Introduction to Fluid Dynamics*, Cambridge Mathematical Library (Cambridge University Press, 1967) pp. 211–216.
- [2] U. Frisch, Symmetries and conservation laws, in *Turbulence: The Legacy of A.N. Kolmogorov*, Cambridge University Press (Cambridge University Press, 1995) pp. 17–18.
- [3] C. Nore, M. Abid, and M. E. Brachet, Kolmogorov turbulence in low-temperature superflows, *Phys. Rev. Lett.* **78**, 3896 (1997).
- [4] T. Araki, M. Tsubota, and S. K. Nemirovskii, Energy spectrum of superfluid turbulence with no normal-fluid component, *Phys. Rev. Lett.* **89**, 145301 (2002).
- [5] M. Kobayashi and M. Tsubota, Kolmogorov spectrum of superfluid turbulence: Numerical analysis of the Gross-Pitaevskii equation with a small-scale dissipation, *Phys. Rev. Lett.* **94**, 065302 (2005).
- [6] A. N. Kolmogorov, Dissipation of Energy in Locally Isotropic Turbulence, *Akademiia Nauk SSSR Doklady* **32**, 16 (1941).
- [7] L. Galantucci, E. Rickinson, A. W. Baggaley, N. G. Parker, and C. F. Barenghi, Dissipation anomaly in a turbulent quantum fluid, *Physical Review Fluids* **8**, 034605 (2023).
- [8] K. W. Schwarz, Three-dimensional vortex dynamics in superfluid ^4He : Line-line and line-boundary interactions, *Phys. Rev. B* **31**, 5782 (1985).
- [9] A. L. Fetter, Vortices in an imperfect Bose Gas. IV. translational velocity, *Phys. Rev.* **151**, 100 (1966).
- [10] K. Sasaki, N. Suzuki, and H. Saito, Bénard–von Kármán vortex street in a Bose-Einstein condensate, *Phys. Rev. Lett.* **104**, 150404 (2010).
- [11] W. J. Kwon, J. H. Kim, S. W. Seo, and Y. Shin, Observation of von Kármán vortex street in an atomic superfluid gas, *Phys. Rev. Lett.* **117**, 245301 (2016).

- [12] L. Onsager, Introductory talk, in *International conference of theoretical physics*, Science Council of Japan, Tokyo (1953) pp. 977–880.
- [13] M. T. Reeves, T. P. Billam, B. P. Anderson, and A. S. Bradley, Identifying a superfluid Reynolds number via dynamical similarity, *Phys. Rev. Lett.* **114**, 155302 (2015).
- [14] Note, we choose $\kappa = \hbar/m$, consistent with our choice of natural units, instead of the conventional $\kappa = h/m$. This results in a transition to turbulence at $\text{Re}_S \sim 1$.
- [15] W. Schoepe, Superfluid Reynolds number and the transition from potential flow to turbulence in superfluid ^4He at millikelvin temperatures, *JETP Letters* **102**, 105 (2015).
- [16] H. Takeuchi, Quantum viscosity and the Reynolds similitude of a pure superfluid, *Phys. Rev. B* **109**, L020502 (2024).
- [17] T. P. Billam, M. T. Reeves, B. P. Anderson, and A. S. Bradley, Onsager-Kraichnan condensation in decaying two-dimensional quantum turbulence, *Phys. Rev. Lett.* **112**, 145301 (2014).
- [18] J. R. Abo-Shaeer, C. Raman, J. M. Vogels, and W. Ketterle, Observation of vortex lattices in Bose-Einstein condensates, *Science* **292**, 476 (2001).
- [19] T. W. Neely, E. C. Samson, A. S. Bradley, M. J. Davis, and B. P. Anderson, Observation of vortex dipoles in an oblate Bose-Einstein condensate, *Phys. Rev. Lett.* **104**, 160401 (2010).
- [20] W. J. Kwon, G. Moon, S. W. Seo, and Y. Shin, Critical velocity for vortex shedding in a Bose-Einstein condensate, *Phys. Rev. A* **91**, 053615 (2015).
- [21] L. Pitaevskii and S. Stringari, *Bose-Einstein Condensation* (Clarendon Press, 2003) Chap. 5.4, pp. 47–52.
- [22] S. Hoerner, *Fluid-dynamic Drag: Practical Information on Aerodynamic Drag and Hydrodynamic Resistance* (Hoerner Fluid Dynamics, 1965).
- [23] A. Roshko, *On the development of turbulent wakes from vortex streets*, Tech. Rep. (1954).
- [24] S. Goldstein, *Modern Developments in Fluid Dynamics: An Account of Theory and Experiment Relating to Boundary Layers, Turbulent Motion and Wakes*, Modern Developments in Fluid Dynamics No. v. 2 (Clarendon Press, 1938).
- [25] A. Kaskas, Berechnung der stationären und instationären Bewegung von Kugeln in ruhenden und strömenden Medien, Universität Berlin (West) (1964).
- [26] S. Babuin, E. Varga, L. Skrbek, E. Lévêque, and P.-E. Roche, Effective viscosity in quantum turbulence: A steady-state approach, *Europhysics Letters* **106**, 24006 (2014).
- [27] G. Stokes, On the effect of internal friction of fluids on the motion of pendulums, *Transaction of the Cambridge Philosophical Society* **9**, 120 (1851).
- [28] The cylindrical obstacle has a small correction to the value of α , as described by Lamb in [29].
- [29] H. Lamb, XV. On the uniform motion of a sphere through a viscous fluid, *The London, Edinburgh, and Dublin Philosophical Magazine and Journal of Science* **21**, 112 (1911).
- [30] T. Frisch, Y. Pomeau, and S. Rica, Transition to dissipation in a model of superflow, *Phys. Rev. Lett.* **69**, 1644 (1992).
- [31] L. Prandtl, *Verhandlungen des dritten Internationalen mathematikerkongresses in Heidelberg: vom 8. bis 13. august 1904* (BG Teubner, 1905) p. 484.
- [32] H. Blasius, Grenzschichten in flüssigkeiten mit kleiner reibung., *Zeitschrift für Angewandte Mathematik und Physik* **56**, 1 (1908).
- [33] G. W. Stagg, N. G. Parker, and C. F. Barenghi, Superfluid boundary layer, *Phys. Rev. Lett.* **118**, 135301 (2017).
- [34] T. Frisch, S. Nazarenko, and S. Rica, Superflow passing over a rough surface: Vortex nucleation, *Phys. Rev. Fluids* **9**, 024701 (2024).
- [35] D. C. Jespersen, T. H. Pulliam, and M. L. Childs, *OVERFLOW Turbulence Model Resource Verification Results*, Tech. Rep. (2016).
- [36] Y. A. Çengel and J. M. Cimbala, *Fluid mechanics fundamentals and applications* (McGraw-Hill Education, 2018) Chap. 4, 6, pp. 164–169, 250–257.
- [37] N. Nangia, H. Johansen, N. A. Patankar, and A. P. S. Bhalla, A moving control volume approach to computing hydrodynamic forces and torques on immersed bodies, *Journal of Computational Physics* **347**, 437 (2017).
- [38] O. Reynolds, On the sub-mechanics of the universe, *Proceedings of the Royal Society of London* **69**, 425 (1902).
- [39] T. Winiecki, B. Jackson, J. McCann, and C. Adams, Vortex shedding and drag in dilute Bose-Einstein condensates, *Journal of Physics B: atomic, molecular and optical physics* **33**, 4069 (2000).
- [40] N. Navon, A. L. Gaunt, R. P. Smith, and Z. Hadzibabic, Emergence of a turbulent cascade in a quantum gas, *Nature* **539**, 72 (2016).
- [41] S. W. Seo, B. Ko, J. H. Kim, and Y. Shin, Observation of vortex-antivortex pairing in decaying 2D turbulence of a superfluid gas, *Scientific Reports* **7**, 4587 (2017).

Supplemental Material for: Emergent Universal Drag Law in a Model of Superflow

M.T.M. Christenhusz,¹ A. Safavi-Naini,² H. Rubinsztein-Dunlop,¹ T.W. Neely,¹ and M.T. Reeves³

¹*Australian Research Council Centre of Excellence for Engineered Quantum Systems,
School of Mathematics and Physics, University of Queensland, St. Lucia, QLD 4072, Australia.*

²*Institute of Physics, University of Amsterdam, Science Park 904, 1098 XH Amsterdam, the Netherlands.*

³*Australian Research Council Centre of Excellence in Future Low-Energy Electronics Technologies,
School of Mathematics and Physics, University of Queensland, St Lucia, QLD 4072, Australia.*

(Dated: June 21, 2024)

METHOD

To model our wake, we cast the Gross-Pitaeskkii equation (GPE) into a moving frame. To prevent re-entry of vortices, we apply a fringe region on the edges of the computational grid. This region is represented by the damping, $\gamma(\mathbf{r})$, in Eq. 3 in the main text and is given by,

$$\begin{aligned}\gamma(\mathbf{r}) &= \max[\gamma(x), \gamma(y)] \quad \text{with} \\ \gamma(i) &= \frac{\gamma_0}{2} \left[2 + \tanh\left(\frac{i - w_i}{d}\right) - \tanh\left(\frac{i + w_i}{d}\right) \right]\end{aligned}\tag{S1}$$

where $i \in \{x, y\}$, $d = 7\xi$, $w_i = 0.4L_i$ and $\gamma_0 = 0.25$. The potential $V(\mathbf{r})$ is contained inside \mathcal{L} (Eq. 2) and have analytic definitions for the hard-wall and Gaussian obstacle:

$$V_{HW}(\mathbf{r}) = \frac{V_0}{2} \left[\tanh\left(\frac{r - \sigma}{2}\right) + \tanh\left(\frac{r + \sigma}{2}\right) \right]\tag{S2}$$

$$V_G(\mathbf{r}) = \frac{V_0}{2} \exp(-r^2/\sigma^2),\tag{S3}$$

where $\sigma = D/2\xi$ and $r = \sqrt{(x - x_0)^2 + y^2}$. The labels HW and G correspond to cylinder and Gaussian, respectively.

Our study is performed on a grid of sufficient size, while considering computation speed. A sufficiently large grid ensures no edge effects such as reflections interfere with the wakes. Working in units of healing length, ξ , speed of sound, $c = \sqrt{\mu/m}$ and time $\tau = \hbar/\mu$, a spatial grid of the size $L_x = 512\xi$ by $L_y = 256\xi$ was found to be sufficiently large for barrier sizes up to $D = 24\xi$, whilst maintaining sufficient computational speed. The computational grid is $M_x = 2L_x$ by $M_y = 2L_y$, providing two grid points per healing length.

SUPERFLUID DRAG COEFFICIENT

The superfluid drag coefficient is introduced in the main text as $C_{d_s} = 2F_d/\rho(u^2 - u_c^2)D$. We justify how this drag coefficient is established by considering the drag force in context of the dynamic pressure. The drag equation is given by $F_d = qC_dD$, with D the obstacle size, C_d the drag coefficient and $q = \frac{1}{2}\rho u^2$ the dynamic pressure. The drag depends linearly on the dynamic pressure and becomes nonzero for $u > 0$.

Due to an absence of superfluid drag below the object dependent critical velocity, u_c , it is useful to introduce a superfluid dynamic pressure such that the drag equation becomes nonzero at the critical velocity:

$$q_s = q - q_c = \frac{1}{2}\rho u^2 - \frac{1}{2}\rho u_c^2 = \frac{1}{2}\rho(u^2 - u_c^2).\tag{S4}$$

Substituting this into the drag equation and solving for the drag coefficient leads to the superfluid drag coefficient,

$$C_{d_s} = \frac{2F_d}{\rho(u^2 - u_c^2)D}.\tag{S5}$$

DRAG COEFFICIENT FITTING

To obtain the coefficients α and β in Eq. 4 of the main text, the asymptotic value a_0 was subtracted to find the appropriate power laws. To find a power law through fitting linear functions on logarithmic axes, care must be taken to subtract any asymptotic offset: The gradient of the linear fit is not representative of data due to the logarithmic identity $\log(C_{d_S} - a_0) = \log \text{Re}_S^\alpha = \alpha \log \text{Re}_S$, rather than $\log C_{d_S} = \log(\text{Re}_S^\alpha + a_0)$, which has no logarithmic identity. A result of the subtraction of a_0 is that points where $C_{d_S} - a_0 \rightarrow 0$, data deviates much more and a collapse onto a single curve seems less apparent. Figure S1 is an addition to Fig. 2 of the main text, where we demonstrate the collapse onto a single curve on logarithmic axes without subtracting the asymptotic offset. For both the (a) hard-walled obstacle and (b) Gaussian obstacle, this effect is most pronounced around $\text{Re}_S \sim 10^1$, with the points on this plot appearing to follow a power law much more closely here.

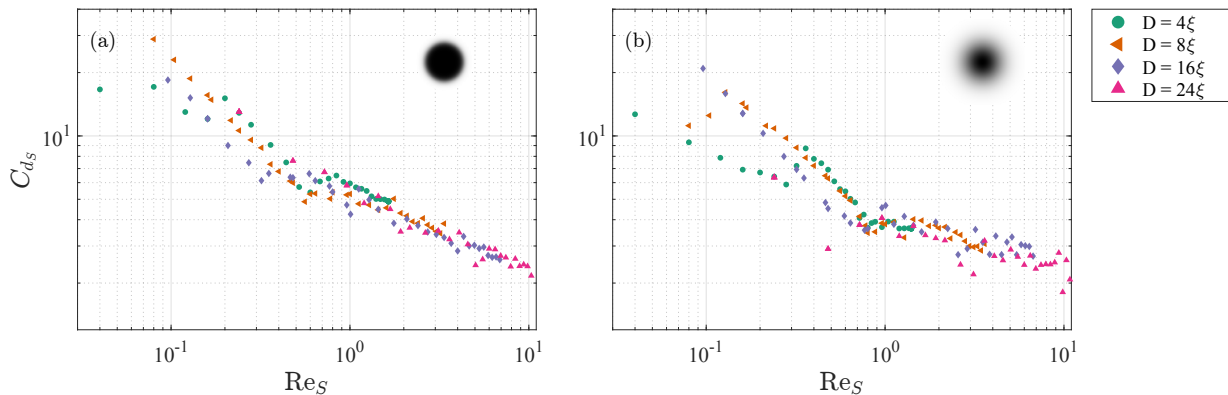


FIG. S1. Drag coefficient on log-log axes without subtracting a_0 , as is done in the insets in Fig. 2 of the main text. To obtain the correct coefficients α and β , the asymptotic value a_0 must be subtracted. Without subtracting, the power laws appear to collapse better onto a single curve as can be seen for the (a) hard-walled and (b) Gaussian obstacle.

DRAG COEFFICIENTS OF NONTRIVIAL GEOMETRIES

Table I shows the (superfluidic) drag coefficients for all obstacle shapes, including the wedge, flat plate and airfoil. The drag coefficient given is $C_{d_S}(\text{Re} \rightarrow \infty) = a_0$, obtained through the method described in the main text. To obtain the coefficient and show the further extend of the dynamical similarity, the superfluid drag coefficient is plotted as a function of the superfluid Reynolds number in Fig S2.

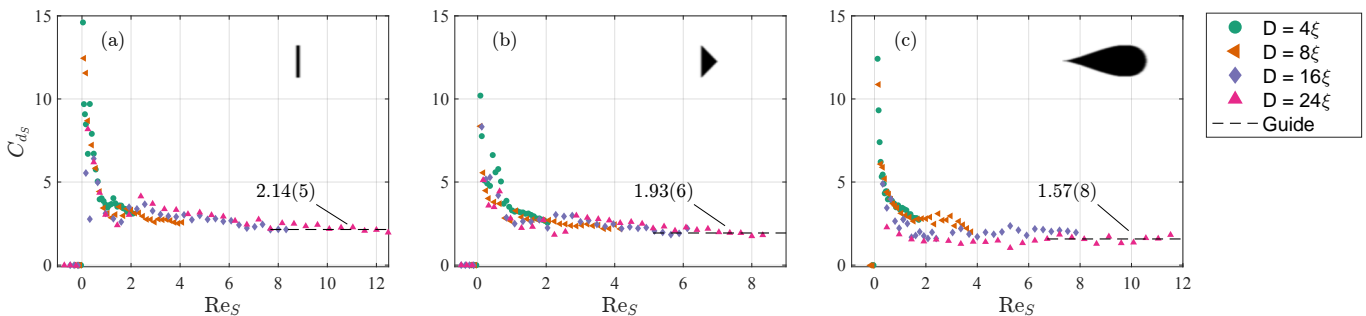


FIG. S2. Drag coefficient as a function for the Reynolds number for the (a) flat plate, (b) wedge and (c) airfoil. The angle of attack is from right to left. The dashed lines correspond with guide lines corresponding with the obtained a_0 coefficient.